



Kahramanmaraş Sutcu Imam University Journal of Engineering Sciences



Geliş Tarihi : 12.10.2023
Kabul Tarihi : 08.11.2023

Received Date : 12.10.2023
Accepted Date : 08.11.2023

MIXED MODE FRACTURE OF THE GEOPOLYMER COMPOSITES REINFORCED WITH RECYCLED STEEL FIBERS

ATIK ÇELİK LİFLERLE GÜÇLENDİRİLMİŞ GEOPOLİMER BETONLARDA KARIŞIK MOD KIRILMASI

Muhammed GÜMÜŞ^{1*} (ORCID: 0000-0002-7380-0098)
Hakan BAYRAK¹ (ORCID: 0000-0001-9441-2214)

¹ Kafkas Üniversitesi, İnşaat Mühendisliği Bölümü, Kars, Türkiye

*Sorumlu Yazar / Corresponding Author: Muhammed GÜMÜŞ, muhammedgumus@kafkas.edu.tr

ABSTRACT

For the fiber-reinforced composites, strength-based criteria alone may fail to evaluate the bending response due to the long tail of the load-displacement curve. Hence, the fracture characterization of fibered composites has gained great attention worldwide. In this study, the mixed-mode fracture performance of the recycled steel fiber-reinforced geopolymer concrete was examined experimentally. The main test parameters were the amount of steel fibers (0 and 2% by mass) and the offset ratios of the edge notch ($\beta = 0, 0.2, \text{ and } 0.4$). Several notched prisms were produced and tested under a deformation-controlled three-point bending test. Deformation maps on the surface of the specimens were derived through the digital image correlation method. Experimental results were discussed concerning the first cracking load, ultimate load, critical crack mouth opening displacement, critical crack mouth sliding displacement, and fracture energy. Based on the experimental findings, it can be stated that the peak flexural loads were increased by 666%, 1327%, and 400%, respectively for the 0, 0.2, and 0.4 notch offset ratios due to the use of recycled steel fiber. The fracture energies of the plain specimens were proportional to the notch offset ratio, but they fluctuated for the fiber-reinforced specimens because of the uneven distribution of fibers.

Keywords: Fracture mechanics, recycled steel fiber, geopolymer, digital image correlation

ÖZET

Yük deplasman eğrisinin uzun kuyruk kısmından dolayı, çelik lifli kompozitlerin eğilme davranışının değerlendirilmesinde dayanım kriteri tek başına doğru bir değerlendirme için yeterli değildir. Bu nedenle, lifli kompozitlerin kırılma karakterleri dünya genelinde giderek önem kazanmaktadır. Mevcut çalışmada, atık çelik liflerle güçlendirilmiş geopolimer betonların Mod-II kırılma performansı deneysel olarak incelenmiştir. Çalışmadaki temel parametreler çelik lif miktarı (kütlece %0 ve %2) ve çentik öteleme oranlarıdır ($\beta = 0, 0.2 \text{ ve } 0.4$). Çok sayıda çentikli numuneler üretilmiş ve deformasyon kontrollü üç noktalı eğilme deneyi ile test edilmiştir. Eleman yüzeylerindeki deformasyon dağılımları dijital görüntü korelasyonu metodu ile hesaplanmıştır. Elde edilen sonuçlar ilk çatlama yükü, maksimum yük, kritik çatlak ağzı açılma deplasmanı, kritik çatlak ağzı kayma deplasmanı ve kırılma enerjisi açısından irdelenmiştir. Elde edilen deneysel sonuçlardan, kullanılan çelik liften dolayı maksimum eğilme yükünün 0, 0.2, ve 0.4 çentik öteleme oranlarında sırasıyla 666%, 1327%, ve 400% arttığı görülmüştür. Lif içermeyen elemanların kırılma enerjisi çentik öteleme oranıyla doğrusal olarak değişmekteyken, çelik liflerin homojen olmayan dağılımından dolayı lifli elemanların kırılma enerjisinde dalgalanmalar görülmüştür.

Anahtar Kelimeler: Kırılma mekaniği, atık çelik lif, geopolimer, dijital görüntü korelasyonu

INTRODUCTION

The annual carbon dioxide emissions caused by the cement-related sectors worldwide were recorded as approximately 1.5 billion tons which corresponds to 6% of the total toxic gasses emissions (Amran et al., 2020). As an alternative to ordinary Portland cement-based concrete, geopolymers have been known as green concretes due to their cement-free mixture compositions. Their strength arises from the amorphous inorganic polymeric chains as a result of chemical reactions between the aluminosilicate precursors and the alkaline solutions. The by-product or waste materials such as slag, fly ash, metakaolin, silica fume, red mud, glass powder, and rice husk are the main sources of the aluminosilicate precursors (Almutairi et al., 2021). The hardened state of the geopolymers shows superior mechanical and durability properties compared to ordinary cement-based concrete (Ding et al., 2016). Unfortunately, due to the highly amorphous intrinsic structures, brittleness remains a matter for the geopolymer concretes. To overcome that issue, the fibers were dispersed into the mixtures in the fresh state. The pioneering study on the reinforcing of geopolymers was conducted by Davidovits (Davidovits, 1991). Since then, several types of fibers have been applied to improve the brittle characteristics of the geopolymer concretes (Laxmi & Patil, 2022; Ranjbar & Zhang, 2020). Among all the fibers, the most preferred type was the steel fibers with various geometric shapes (Rashad, 2020).

The contribution of the dispersed steel fibers to the crack bridging almost occurred at the post-peak region of the bending response. The main reason is that the fibers are activated following the initial formation of the cohesive crack. Hence, the stress-based criteria may alone lead to a misleading interpretation of the fracture evaluation of fiber-reinforced concrete (Shi et al., 2020). In literature, most of the ongoing research worldwide has been focused on the fracture behavior of industrial steel fiber-reinforced geopolymer composites. Aisheh et al. (Aisheh et al., 2022) reported that the steel fibers improve the fracture energy and stress intensity factor of ultra-high performance geopolymer composites. Zang et al. (Zhang et al., 2021) declared that the initial and the unstable fracture toughness of the plain geopolymer concrete is enhanced by 27.8% and 12.74-fold, respectively, thanks to steel fiber usage at 2.5 vol%. Implementing the work of fracture and the size effect method, Mousavinejad and Gashti (Mousavinejad & Gashti, 2021) revealed the correlation between steel fibers and the fracture characteristics of the heavyweight geopolymer concretes. Liu et al. (Liu et al., 2020) stated that although the increase in the steel fiber content up to 2 vol% significantly amends both fracture properties of the geopolymer concrete, further rise in the fiber content has a limited effect on the increment in the fracture energy. Gomes et al. (Gomes et al., 2020) pointed out the conversion from unstable to stable crack growth due to the utilization of steel fibers in geopolymer mixtures. They also specified the optimum fiber dosages of 0.5 vol% at which all the fracture parameters investigated reached the peak values. Similarly, the improvement in fracture characteristics is also stated in the experimental studies (Al-Rawi & Taysi, 2018; Ding & Bai, 2018). Briefly, as observed from the experimental findings given above, the industrial steel fibers positively affect the fracture parameters of the geopolymer concretes.

On the other hand, the philosophy of the invention of the geopolymer concretes seems to conflict with the use of industrial steel fibers. The global warming potential of industrial steel fibers is 1095.88 kgCO₂/ton which is even higher than that of the 903.23 kgCO₂/ton for ordinary Portland cement (Frazão et al., 2022). Compared to industrial steel fibers, the recycled steel fibers from the end-of-life tires have only 54.74 kgCO₂ per one-ton raw material production (Frazão et al., 2022), which means a 95% reduction in greenhouse gas emissions. Within this perspective, researchers aim to substitute industrial steel fiber with recycled one. The scope of the research attempts could be divided into three categories: (i) fresh (Celik & Ozkilic, 2023; Eskandarinia et al., 2022; Zhong et al., 2019), (ii) mechanical (Celikten, 2022; Mucsi et al., 2018; Yolcu et al., 2022) and (iii) durability and transport properties (Althoey et al., 2023) of the recycled steel fiber reinforced geopolymers. In some cases, recycled steel fibers were hybridized with industrial steel fibers (Alsaif & Albidah, 2022) or polyvinyl alcohol (Wang et al., 2020) to benefit from the synergetic effect of fibers. In most studies, the mechanical characteristics such as flexural and compressive strength as well as the fresh state features were well examined.

As observed from the literature review, the experimental research on the geopolymer concretes failed to address the fracture performance of the recycled steel fiber-reinforced composites. Thus, the aim of the present study was to shed new light on the effect of recycled steel fibers on the Mode-II fracture behavior of geopolymer composites. The main parameters of the study were the notch offset ratios ($\beta = 0, 0.2, \text{ and } 0.4$) and fiber content (0 and 2% by mass). By using the plain mixture and the companion recycled fiber-reinforced composite, a total of 6 prisms with a dimension of 100x100x400 mm were produced. All the specimens were tested under deformation-controlled quasi-static three-point bending loads. The formation and propagation of the cohesive crack were recorded through the two-dimensional

digital image correlation method. Test results were inspected in terms of (i) first cracking load, (ii) ultimate load, (iii) critical crack mouth opening, $CMOD_c$, (iv) critical crack mouth sliding displacement, $CMSD_c$, and (v) fracture energy. Despite the limited number of samples, we believe that the findings would be useful to extend the current knowledge about recycled fiber-reinforced geopolymers.

EXPERIMENTAL PROCEDURES

Raw Materials

As an aluminosilicate source material, ground granulated blast-furnace slag was utilized in the mixture. The specific gravity and the specific surface of the slag were reported by the manufacturer as 2.9 g/cm^3 and $5445 \text{ cm}^2/\text{g}$, respectively. Marble powder was intentionally chosen as a filler material due to environmental concerns. The particle size of the marble powder varied between 0-400 microns. Besides the marble powder, no additional coarse or fine aggregate was used in the mixture. To activate the aluminosilicate precursor, sodium silicate and sodium hydroxide solution were employed. The concentration ratios of the sodium silicate and sodium hydroxide solutions were 36% and 48%, respectively. The molarity of the sodium hydroxide was 12 M. The density of the sodium silicate and sodium hydroxide solutions was approximately 1.38 g/cm^3 . Aiming the environmental benefits, recycled steel fibers were incorporated into the concrete mixtures. Peak frequency of about 10% in fiber length corresponded to the range of 24-28 mm. Figure 1 shows a physical representation of the ingredients used to produce geopolymer composites.



Figure 1. Raw Materials Used for Manufacturing Geopolymer Composites

Manufacturing Test Specimen

Table 1 presents the ingredients used for the geopolymer composites. As given in the table, the precursor to the activator (sum of sodium silicate and sodium hydroxide) ratio was equal to 2. The sodium silicate to the sodium hydroxide ratio was 2.5. Those ratios were set as constant for each mixture. However, for the volume stability of the mixture, the amount of the marble powder was changed between 311 and 327 kg/m^3 . As for the fiber-reinforced composites, 46 kg of recycled steel fiber was included in the fresh mixture, which corresponded to about 2% by mass. The concrete mixtures were entitled according to their fiber content. “P” and “F” in Table 1 stand for the plain and the fiber-reinforced geopolymer composites.

Table 1. The Mixture Compositions for the Geopolymer Concretes (kg/m^3)

| Mix ID | Slag | Marble powder | Sodium silicate | Sodium hydroxide | Steel fiber | Total mass (kg) |
|--------|------|---------------|-----------------|------------------|-------------|-----------------|
| P | 1260 | 327 | 450 | 180 | 0 | 2217 |
| F | 1260 | 311 | 450 | 180 | 46 | 2247 |

To increase the homogeneity of the mixture, slag, and the marble powder were first blended in a dry condition for one minute. Then, the liquid solution comprising sodium silicate and sodium hydroxide was added to the dry mixture and continued to blend for another four minutes. In the case of steel-fibered concretes the recycled steel fibers were incorporated into the fresh mixture. While adding steel fibers, particular attention was paid to preventing the fiber balling. Fibers were dispersed into the mixture slowly during the mixing for the next one minute. Fresh mixtures were cast into the wooden molds with a clear dimension of $100 \times 100 \times 400 \text{ mm}^3$. The open surface of the molds was covered with a thin plastic sheet to prevent evaporation. Approximately 24 hours following the casting, specimens were demolded and submerged into the water tank to apply a water cure during the testing day.

Before the experiments, the specimens were cut through the circular concrete saw to open an edge notch perpendicular to the longitudinal axis of the specimens. Notch depth was constant for each specimen and equal to 30 mm. However, the notch offset ratios, which were defined as the offset distance from the center to the half of the distance between supports, were 0, 0.2, and 0.4. Accordingly, the notch distances were 0, 30, and 60 mm, respectively from the specimen center. Figure 2.a. illustrates the distribution of the notch locations on the specimen surfaces. In this work, the deformation levels on the specimen surface were obtained by using the two-dimensional digital image correlation method. To this end, the surface of the specimens was first painted white and then the speckle patterns were created on the white background. The notched prisms were named according to their concrete and the offset ratio. For instance, the specimen designated by “P-0.2” has a plain geopolymer concrete and a notch offset ratio of 0.2, respectively.

Installing Test Set up

Figure 2.b demonstrates a representative view of the experimental arrangement used in the present work. As observed from the figure, the specimen's clear span length was adjusted to 300 mm, which yielded a span-to-depth ratio of 3. Notched beams were exposed to a deformation-controlled bending load. For the plain specimens, the loading rate was 0.2 mm/minute and constant during the experiment. In the case of fiber-reinforced specimens, loading rates were increased step by step up to the complete failure of the specimen. 0.2 mm/minute loading rate was applied between the stroke length of 0-0.6 mm. It suddenly increased to 1.0 mm/minute and 2.0 mm/minute when the stroke length of the testing machine exceeded 0.6 mm and 4.5 mm deflection, respectively. Data for the load exposed were determined by the load cell mounted on the loading machine and were recorded by using computer software. The vertical and the horizontal deformation maps on the specimen surface were calculated from the sequentially deformed images. To this end, the distorted shapes of the specimen, which are not possible to detect by the naked eye, were captured during the experiment at a time interval of 3 seconds. A Canon 6D Mark II digital camera and a Canon 50 mm f/1.4 USM lens were used for the image recording. To increase the contrast between the white background and the dots on it, LED light sources were operated. Those assemblies are also given in Figure 2. b. In this study, the image resolution was approximately equal to 14 pixels/mm. Images were analyzed by using an open-source algorithm developed by (Blaber et al., 2015). The analysis parameters such as subset size, subset spacing, and the strain radius were adjusted to 35, 15, and 5 pixels, respectively.

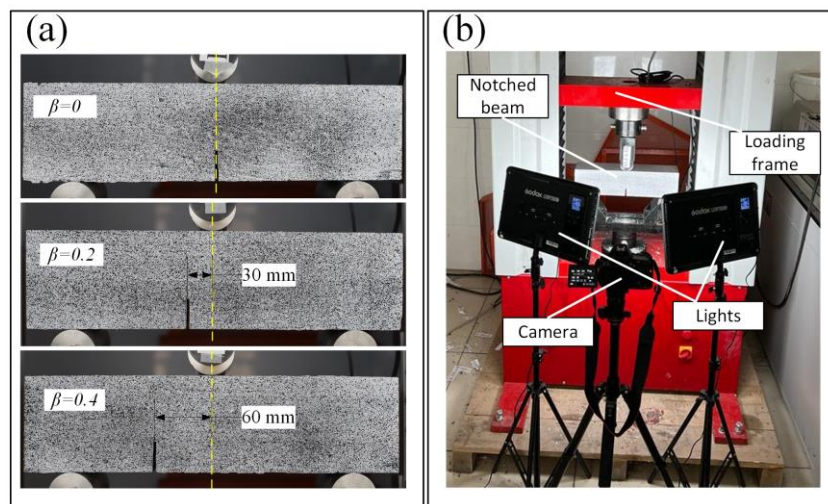


Figure 2. a. Notch Offset Distance b. Test Setup and Measurement Devices

RESULTS and DISCUSSIONS

Initial Cracking Load

Initial cracking loads were of significance to separate the complete elastic and elastic-plastic behavior of a material exposed to external loading. However, the determination of the first cracking point from the load versus deflection curves was a matter requiring a qualified perspective. Hence, strain gauges fixed on the notched tip were frequently employed for defining that bifurcation point. In this work, on the other hand, CMODs-Times graphs as in Figure 3 were handled to specify that transition point. From the figure, the first lateral region of the curves corresponded to the elastic behavior and thereby the end point of that plateau represented the cracking point of the specimen. Although the loading rates of the plain specimens were the same as those of the fiber-reinforced specimens, the fracture

initiation in the plain specimens was formed before the fiber-reinforced specimens. Initial cracking time is 114, 138, 150, 198, 183, and 177 s, respectively for the P-0, P-0.2, P-0.4, F-0, F-0.2, and F-0.4 specimens.

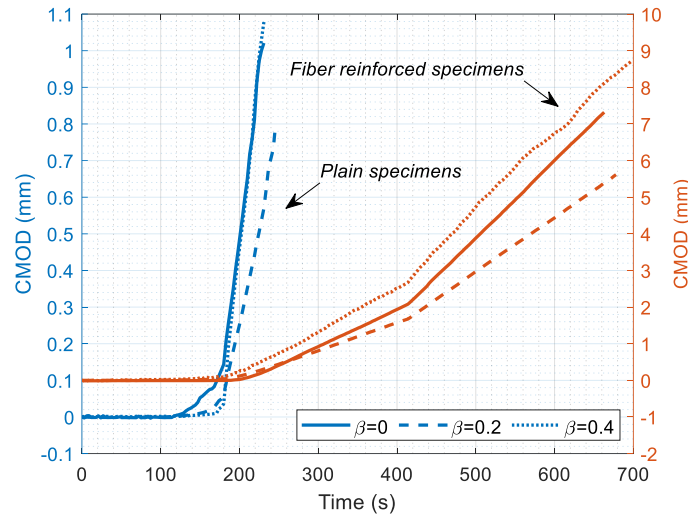


Figure 3. Comparison Between CMOD-time Curves of Plain and Fibered Geopolymers

A similar conclusion was also achieved in terms of the cracking loads. As seen in Table 2, compared to the fiber-reinforced specimens, plain specimens had lower cracking load capacities for each case of the notch offset ratios. The increment in the cracking load capacity due to recycled fiber usage was approximately 636.6%, 1251.1%, and 290.7% respectively for the offset ratio of 0, 0.2, and 0.4. Such an experimental finding conforms to the literature (Ahmad et al., 2021) in which the initial cracking load of ordinary concrete increased with the increasing steel fiber content. Accordingly, such an improvement may be referred to as the bridging mechanism of the steel fibers dispersed throughout the cohesive zone of the concrete. The other significant outcome from the experiments could be attained by examining the offset ratios. In the case of plain specimens, when it ascended from 0 to 0.2 and 0.4, the initial cracking loads first slightly changed and then significantly raised by about 148.2%. For the fiber-reinforced specimens, the improvement in the cracking load capacity was by about 51.4% and 31.1% due to the offset ratio of 0.2 and 0.4, respectively. Accordingly, it can be inferred that each test parameter influenced the initial cracking load though, the recycled fiber effect on the cracking load was much more dominant than that of the notch offset ratio.

Table 2. Some Mechanical and Fracture Quantities Measured

| Specimen | Cracking load (N) | Ultimate load (N) | CMOD _c (mm) | CMSD _c * (mm) | G _F (N/mm) |
|----------|-------------------|-------------------|------------------------|--------------------------|-----------------------|
| P-0 | 338.0 | 461.7 | 0.002 | 0.0016 | 0.011 |
| P-0.2 | 280.1 | 393.7 | 0.022 | 0.0100 | 0.027 |
| P-0.4 | 838.9 | 1017.8 | 0.009 | 0.0003 | 0.034 |
| F-0 | 2499.9 | 3536.4 | 0.201 | 0.0628 | 1.639 |
| F-0.2 | 3784.5 | 5618.1 | 0.286 | 0.0312 | 4.097 |
| F-0.4 | 3277.2 | 5088.8 | 0.259 | 0.0909 | 2.763 |

* Absolute magnitude

Ultimate Load

The load-bearing capacity may be referred to as the resisting capacity of a specimen against the load excited and is of significance for the designer. The recorded load-bearing capacities of the notched beams tested are given in Table 2 as well as Figure 4. Accordingly, it can be clearly seen that the recycled steel fibers enhanced the load-bearing capacity of the notched beams irrespective of the offset ratio. Due to the fiber additive at a 2% by mass, bearing capacity was increased by 666%, 1327%, and 400% for the notch offset ratio of 0, 0.2, and 0.4, respectively. This increment in the load-bearing capacity of geopolymer concretes resulting from the fiber additive is in good agreement with the findings in the literature (Celikten, 2022). The fiber bridging in the cohesive zone located in front of the initial notch is the main source of those increments in the load-bearing capacities of the fiber-reinforced specimens. Regarding the test parameters of the offset ratio, bearing capacity variation fluctuated as the offset ratio ascended. For the plain specimens, the peak load was decreased by 14.7% at the 0.2 offset ratio, then increased by 120.4% at the 0.4 offset ratio compared to the zero offset. When the fibered specimens were considered, the peak loads were

improved by 58.9% and 43.9% respectively for the offset ratio of 0.2 and 0.4 compared to the zero offset. Best fit functions for plain and fiber-reinforced specimens were also drawn in Figure 4. The functions indicate the clear increasing trend between the ultimate loads and the offset ratios. In the present work, due to some laboratory limitations, the number of specimens may be insufficient to represent the average value of the test results. Hence, to obtain more accurate results, more specific experimental attempts with a large number of identical specimens are needed in future works.

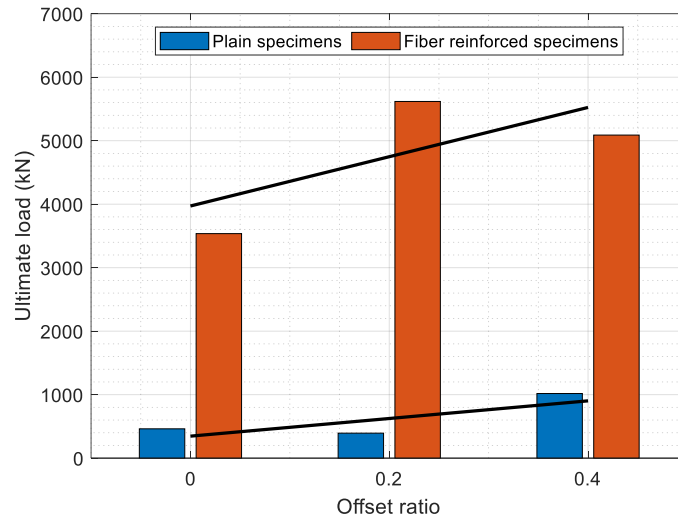


Figure 4. Variation of the Ultimate Load with the Increasing Offset Ratios

Crack Mouth Opening Displacement

For quasi-brittle materials like concretes, the smeared crack approach may result in a misleading evaluation when the cracks were formed. Hence, the crack mouth opening displacement (CMOD) was required to define the stress decay under increasing deflection loading. Figure 5 comparatively displays the load versus CMOD diagrams of the notched beams. From the comparison between Figure 5.a and b, it could be said that fiber addition decelerated the crack growth at the post-peak region, which yielded considerable residual strength levels. It is also significant to declare that the increasing offset ratio provided the notched beams an additional residual strength to some extent. In Figure 5.a, a limited improvement in the residual strength magnitudes could be seen for the plain specimens. However, as in Figure 5.b, the increment in the residual strength in fiber-reinforced geopolymers due to the notch offset ratio was remarkable. These observations were in line with the findings in the literature (Zhong et al., 2019). They pointed out that the increase in the recycled steel fiber content leads to an amendment in the post-peak residual strength levels of geopolymer concretes.

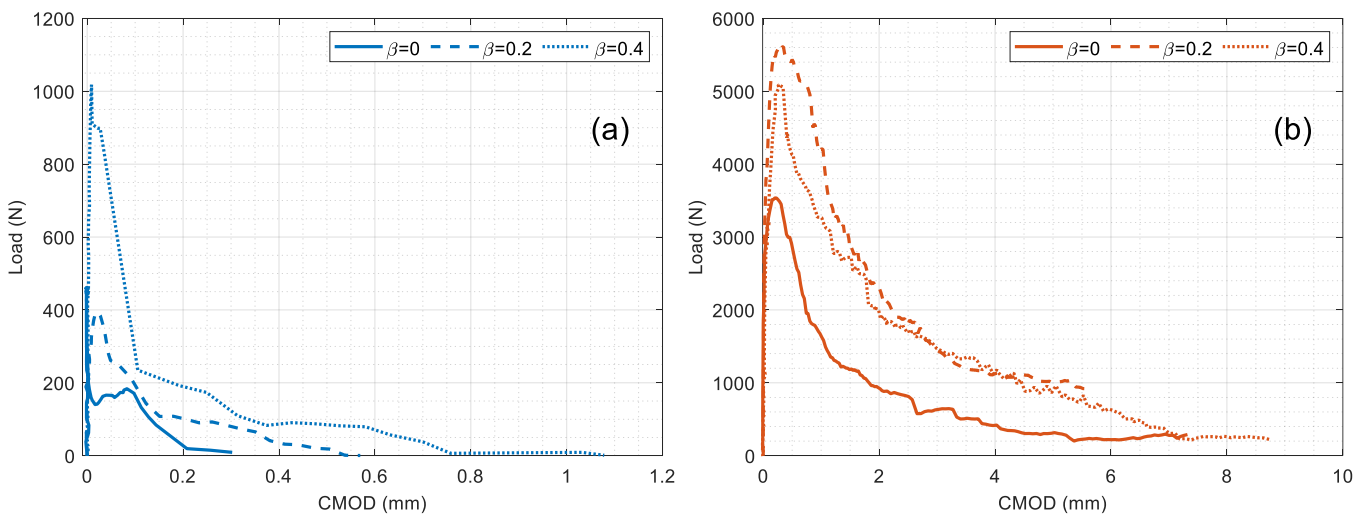


Figure 5. Load Versus CMOD Curves: **a.** Plain and **b.** Fiber Reinforced Specimens

CMODs at the time of peak load is reached are given in Table 2 and also plotted in Figure 6. As is seen from the figure, the offset ratio of 0.2 produced the highest critical CMOD ($CMOD_c$) for both plain and fiber-reinforced

geopolymers. Such a result is also predictable. As the notch offset moves to the support, the specimen's response converts from opening mode (mode-I) to the shear mode (mode-II). At a specific region in the shear span, CMOD is expected to reach its highest magnitudes and then is gradually substituted by CMSD as the notch further moves toward the supports. By comparing the $CMOD_c$ from the fibered and plain specimens, it is obtained that the fiber usage prolonged the critical CMOD at each offset ratio. Besides, the fiber usage also decreased the deviations in the set of $CMOD_c$ values. Differences between the maximum and minimum $CMOD_c$ in plain and fiber-reinforced specimens were 1000% and 42.3%, respectively.

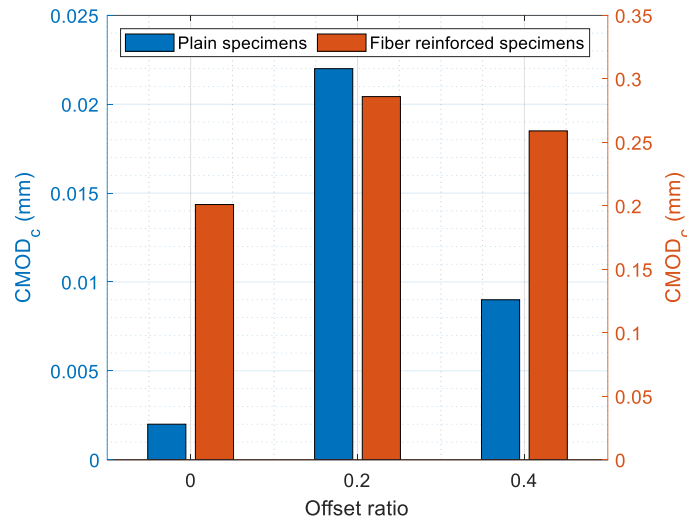


Figure 6. Dependence of the $CMOD_c$ at the Peak Loads on the Offset Ratios

Crack Mouth Sliding Displacement

In many cases, a structural member is subjected to a combined shear and tension stress state. For that reason, the cracking response including sliding and opening may be needed to fairly identify the characteristics of the material investigated. Load versus crack mouth sliding displacements (CMSD) were depicted in Figure 7. It is worth noting that the shear cracking in mixed mode was dominated not only by fiber bridging but also by friction between the crack faces. Hence, the overall shape of the Load-CMSD in Figure 7 could be varied from that of Load versus CMOD in Figure 5. This is because the sliding response in mode-II fracture may not be similar to the Load-CMOD, but it may be noticed by Load-crack tip opening displacement (Nunes & Reis, 2014). In Figure 7.a, strength decay at the post-peak regions seems to be not affected by the notch offset ratio, whereas, for the fiber-reinforced geopolymers in Figure 7.b, the rate of the strength decrements at the same region was depended on the offset ratio. Such a difference could be attributed to the brittleness of the plain specimens. When the first crack was formed at the plain specimens, the main crack sharply developed and did not allow the relative sliding between the crack faces. On the other hand, the recycled steel fibers bridged the crack and caused a slower crack development rate as well as the different sliding options in comparison with the plain specimens.

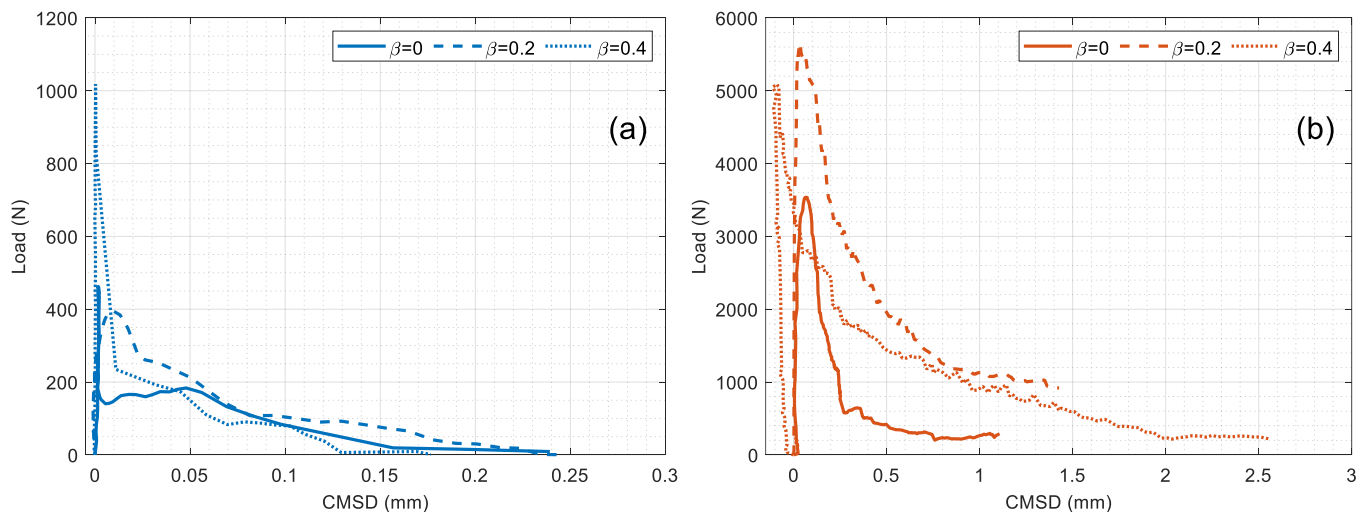


Figure 7. Load Versus CMSD Curves: a. Plain and b. Fiber Reinforced Specimens

The critical magnitude of the CMSD ($CMSD_c$) was obtained for the apex in the load-CMSD curves and given in Table 2 and Figure 8. It is evident from the figure that the fiber inclusion improved the sliding displacement magnitudes of the geopolymers compared to plain specimens. This result was also expected due to the bridging effect of the fibers. Because the fiber addition changes the brittle characteristic of the materials to the ductile one. As a result of such a bridging phenomenon, deviations in $CMSD_c$ of the steel fiber-reinforced geopolymers were much more stable than those of the plain geopolymers. The difference between the highest and lowest values of $CMSD_c$ was by about 3233.3% and 191.3% for the plain and the fiber-reinforced geopolymer specimens.

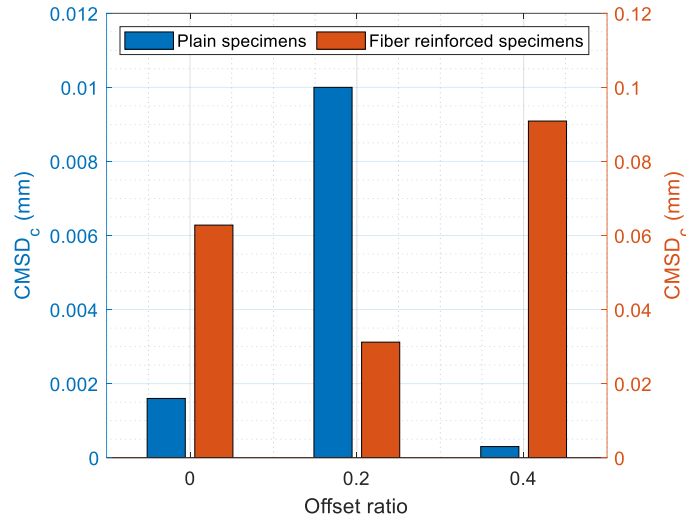


Figure 8. Dependence of the $CMSD_c$ at the Peak Loads on the Offset Ratios

Fracture Energy

Engineering structures have been designed based on the strength criteria of the materials used. However, the fiber-reinforced construction materials were referred to as highly ductile materials due to fiber bridging on the cohesive cracks. Accordingly, the energy-based criteria seem like it might be a more convenient approach in the design of the structures constructed of fiber-reinforced concrete. Figure 9 shows the bending loads applied versus corresponding mid-point deflections. It should be noted here that the net deflections were derived by subtracting the support deflections in this work. Due to the prolonged tail of the fiber-reinforced specimens, their experiments were terminated at about 13 mm deflection value. From the comparison of Figure 9.a and b, it is seen that the residual strength decay was slower in the fiber-reinforced geopolymers, which resulted in a higher fracture energy than the plain specimens.

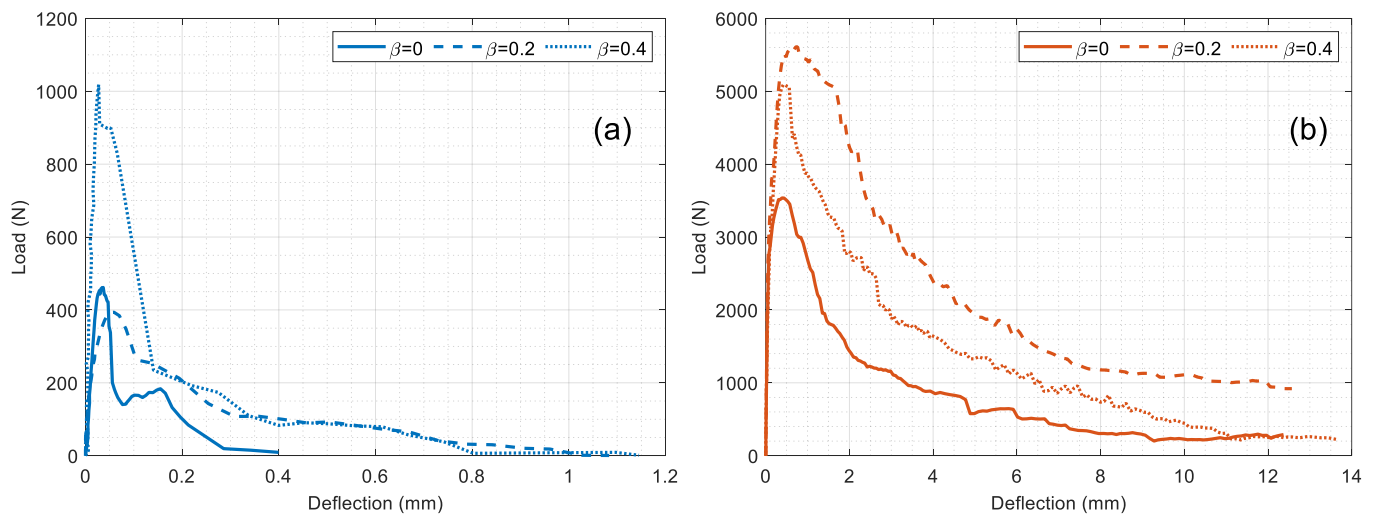


Figure 9. Load Versus Deflection Curves: a. Plain and b. Fiber Reinforced Specimens

The fracture energies were computed by using the following equation (RILEM-Draft-Recommendation, 1985) and then presented in Table 2 and Figure 10.

$$G_F = \frac{W_0 + mg\delta_0}{b(h-a_0)} \quad (1)$$

Where W_0 is the area under the load-deflection curve. m , g , and δ_0 represent the mass of the specimen between the supports, acceleration of gravity, and the ultimate deflection recorded, respectively. b , h , and a_0 stand for the specimen's width and depth, and the initial notch length.

As observed from Figure 10, fracture energies of the plain specimens proportionally increased with the increasing notch offset ratio. This finding conforms to the experimental results in the literature (Nunes & Reis, 2014). They highlighted that the energy release rate (i.e., defined here as the fracture energy) increases as the notch moves the specimen's support point. Comparing Figure 4 and Figure 10, it can be stated that the fluctuation in fracture energy was similar to the fluctuation in the load capacity of fiber-reinforced specimens. Such a result was not surprising because the fracture energy somewhat depended on the both load and the area under the load-deflection curve. In the case of fiber-reinforced geopolymers, the fracture energy initially raised by about 1.5-fold as the offset ratio increased from 0 to 0.2, but then declined to 0.7-fold at the offset ratio of 0.4. Such an unexpected decrement in the fracture energy could be attributed to the heterogeneous distribution of the steel fibers. Eskandarinia et al. (Eskandarinia et al., 2022) stated that the recycled steel fiber at high dosages (i.e., $V_f > 0.6$ vol%) may cause a balling effect due to its irregular shape. Despite the slight decrement in the fracture energy due to the uneven distribution of the fibers, recycled steel fibers significantly amended the fracture energy capacities of the plain geopolymers. When the recycled steel fibers were used, the fracture energies of the plain geopolymers reached 148-fold, 150.7-fold, and 80.3-fold respectively for the 0, 0.2, and 0.4 offset ratios. Therefore, it can be concluded that the recycled steel fiber additive is an effective way to improve the fracture performance of the geopolymer concrete especially for the low fiber dosages (i.e., $V_f < 0.6$ vol%) due to the fiber balling effect.

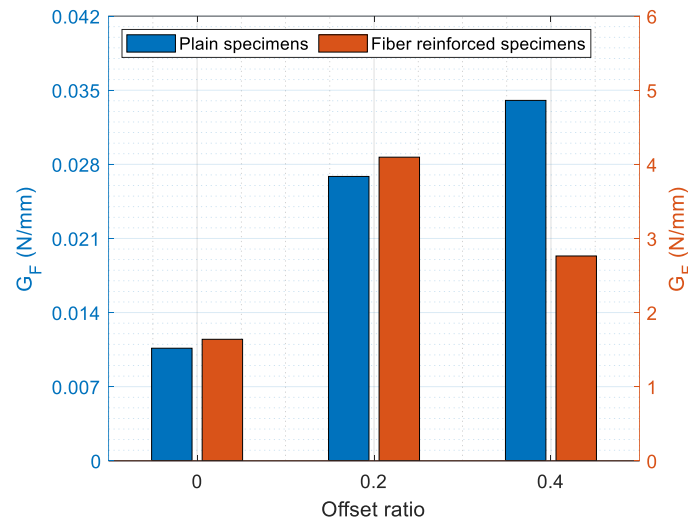


Figure 10. Fracture Energy Variations with the Offset Ratios

CONCLUSIONS

In this work, the effect of recycled steel fibers on the mixed-mode fracture of geopolymer concretes was investigated experimentally. The main test parameters were the recycled steel fiber ratio (0 and 2% by mass) and the notch offset ratio from the center of the specimen (0, 0.2, and 0.4). Notched specimens were subjected to the three-point bending test with a deformation-controlled monotonic loading sequence. The experimental data were recorded by both the software of the testing machine and the images taken by the remote digital camera. Following the experiments, images were analyzed and the surface displacement maps were derived. The main conclusion from the experimental attempt could be summarized as follows:

- The initial cracking load was clearly visible at the CMOD-Time curves. Both the notch offset ratio and fiber content affected the initial cracking load positively. It was also found that the fiber content was much more efficient on the cracking load capacity rather than the notched offset ratio.
- Thanks to the fiber usage at 2% by mass, the peak flexural loads ascended by 666%, 1327%, and 400%, respectively for the 0, 0.2, and 0.4 notch offset ratios.

- Using recycled steel fibers led to an increase in the $CMOD_c$ of notched beams independently of the notched offset ratio. Moreover, randomly disturbed steel fibers helped to decrease the deviations in the $CMOD_c$ values measured such that the variations in $CMOD_c$ of plain specimens were 1000% but only 42.3% for fiber-reinforced specimens.
- Due to the bridging mechanism of the steel fibers, deviations in $CMOD_c$ of the fiber-reinforced specimens were obtained as 191.3%, while it was as high as 3233.3% for the plain specimens.
- In the case of the unreinforced plain specimens, the fracture energies tended to raise proportionally with the notch offset ratio. For the fiber-reinforced specimens, however, the fracture energy increased 1.5-fold for the 0.2 offset ratio, but 0.7-fold for the 0.4 offset ratio compared to the specimens with zero offset.

REFERENCES

- Ahmad, I., Qing, L., Khan, S., Cao, G., Ijaz, N., & Mu, R. (2021). Experimental investigations on fracture parameters of random and aligned steel fiber reinforced cementitious composites. *Construction and Building Materials*, 284, 122680. <https://doi.org/10.1016/j.conbuildmat.2021.122680>
- Aisheh, Y. I. A., Atrushi, D. S., Akeed, M. H., Qaidi, S., & Tayeh, B. A. (2022). Influence of steel fibers and microsilica on the mechanical properties of ultra-high-performance geopolymer concrete (UHP-GPC). *Case Studies in Construction Materials*, 17, e01245. <https://doi.org/10.1016/j.cscm.2022.e01245>
- Al-Rawi, S., & Taysi, N. (2018). Performance of self-compacting geopolymer concrete with and without GGBFS and steel fiber. *Advances in Concrete Construction*, 6(4), 323-344. <https://doi.org/10.12989/acc.2018.6.4.323>
- Almutairi, A. L., Tayeh, B. A., Adesina, A., Isleem, H. F., & Zeyad, A. M. (2021). Potential applications of geopolymer concrete in construction: A review. *Case Studies in Construction Materials*, 15, e00733. <https://doi.org/10.1016/j.cscm.2021.e00733>
- Alsaif, A. S., & Albidah, A. S. (2022). Compressive and flexural characteristics of geopolymer rubberized concrete reinforced with recycled tires steel fibers. *Materials Today: Proceedings*, 65(2), 1230-1236. <https://doi.org/10.1016/j.matpr.2022.04.182>
- Althoey, F., Zaid, O., Alsharari, F., Yosri, A. M., & Isleem, H. F. (2023). Evaluating the impact of nano-silica on characteristics of self-compacting geopolymer concrete with waste tire steel fiber. *Archives of Civil and Mechanical Engineering*, 23, 48. <https://doi.org/10.1007/s43452-022-00587-2>
- Amran, Y. H. M., Alyousef, R., Alabduljabbar, H., & El-Zeadani, M. (2020). Clean production and properties of geopolymer concrete; A review. *Journal of Cleaner Production*, 251, 119679. <https://doi.org/10.1016/j.jclepro.2019.119679>
- Blaber, J., Adair, B., & Antoniou, A. (2015). Ncorr: Open-Source 2D Digital Image Correlation Matlab Software. *Experimental Mechanics*, 55(6), 1105-1122. <https://doi.org/10.1007/s11340-015-0009-1>
- Celik, A. I., & Ozkilig, Y. O. (2023). Geopolymer concrete with high strength, workability and setting time using recycled steel wires and basalt powder. *Steel and Composite Structures*, 46(5), 689-707. <https://doi.org/10.12989/scs.2023.46.5.689>
- Celikten, S. (2022). Properties of recycled steel fibre reinforced expanded perlite based geopolymer mortars. *Advances in Concrete Construction*, 13(1), 25-34. <https://doi.org/10.12989/acc.2022.13.1.025>
- Davidovits, J. (1991). Geopolymers: Inorganic polymeric new materials. *Journal of thermal analysis*, 37(8), 1633-1656. <https://doi.org/10.1007/BF01912193>
- Ding, Y., & Bai, Y. L. (2018). Fracture Properties and Softening Curves of Steel Fiber-Reinforced Slag-Based Geopolymer Mortar and Concrete. *Materials*, 11(8), 1445. <https://doi.org/10.3390/ma11081445>
- Ding, Y., Dai, J.-G., & Shi, C.-J. (2016). Mechanical properties of alkali-activated concrete: A state-of-the-art review. *Construction and Building Materials*, 127, 68-79. <https://doi.org/10.1016/j.conbuildmat.2016.09.121>
- Eskandarinia, M., Esmailzade, M., Hojatkashani, A., Rahmani, A., & Jahandari, S. (2022). Optimized Alkali-Activated Slag-Based Concrete Reinforced with Recycled Tire Steel Fiber. *Materials*, 15(19), 6623. <https://doi.org/10.3390/ma15196623>

- Frazaõ, C., Barros, J., Bogas, J. A., García-Cortés, V., & Valente, T. (2022). Technical and environmental potentialities of recycled steel fiber reinforced concrete for structural applications. *Journal of Building Engineering*, 45, 103579. <https://doi.org/10.1016/j.jobe.2021.103579>
- Gomes, R. F., Dias, D. P., & Silva, F. D. (2020). Determination of the fracture parameters of steel fiber-reinforced geopolymer concrete. *Theoretical and Applied Fracture Mechanics*, 107, 102568. doi:10.1016/j.tafmec.2020.102568
- Laxmi, G., & Patil, S. G. (2022). Effect of fiber types, shape, aspect ratio and volume fraction on properties of geopolymer concrete - A review. *Materials Today: Proceedings*, 65(2), 1086-1094. <https://doi.org/10.1016/j.matpr.2022.04.157>
- Liu, Y. W., Shi, C. J., Zhang, Z. H., Li, N., & Shi, D. (2020). Mechanical and fracture properties of ultra-high performance geopolymer concrete: Effects of steel fiber and silica fume. *Cement & Concrete Composites*, 112, 103665. <https://doi.org/10.1016/j.cemconcomp.2020.103665>
- Mousavinejad, S. H. G., & Gashti, M. F. (2021). Effects of alkaline solution to binder ratio on fracture parameters of steel fiber reinforced heavyweight geopolymer concrete. *Theoretical and Applied Fracture Mechanics*, 113, 102967. <https://doi.org/10.1016/j.tafmec.2021.102967>
- Mucsi, G., Szenczi, A., & Nagy, S. (2018). Fiber reinforced geopolymer from synergetic utilization of fly ash and waste tire. *Journal of Cleaner Production*, 178, 429-440. <https://doi.org/10.1016/j.jclepro.2018.01.018>
- Nunes, L. C. S., & Reis J. M. L. (2014). Experimental investigation of mixed-mode-I/II fracture in polymer mortars using digital image correlation method. *Latin American Journal of Solids and Structures*, 11(2), 330-343. <https://doi.org/10.1590/s1679-78252014000200011>
- Ranjbar, N., & Zhang, M. Z. (2020). Fiber-reinforced geopolymer composites: A review. *Cement & Concrete Composites*, 107, 103498. <https://doi.org/10.1016/j.cemconcomp.2019.103498>
- Rashad, A. M. (2020). Effect of steel fibers on geopolymer properties - The best synopsis for civil engineer. *Construction and Building Materials*, 246, 118534. <https://doi.org/10.1016/j.conbuildmat.2020.118534>
- RILEM-Draft-Recommendation. (1985). Determination of the fracture energy of mortar and concrete by means of three-point bend tests on notched beams. *Materials and Structures*, 18(106), 285-290. <https://doi.org/10.1007/BF02472918>
- Shi, X., Brescia-Norambuena, L., Tavares, C., & Grasley, Z. (2020). Semicircular bending fracture test to evaluate fracture properties and ductility of cement mortar reinforced by scrap tire recycled steel fiber. *Engineering Fracture Mechanics*, 236, 107228. <https://doi.org/10.1016/j.engfracmech.2020.107228>
- Wang, Y., Chan, C. L., Leong, S. H., & Zhang, M. Z. (2020). Engineering properties of strain hardening geopolymer composites with hybrid polyvinyl alcohol and recycled steel fibres. *Construction and Building Materials*, 261, 120585. <https://doi.org/10.1016/j.conbuildmat.2020.120585>
- Yolcu, A., Karakoc, M. B., Ekinci, E., Ozcan, A., & Sagir, M. A. (2022). Effect of binder dosage and the use of waste rubber fiber on the mechanical and durability performance of geopolymer concrete. *Journal of Building Engineering*, 61, 105162. <https://doi.org/10.1016/j.jobe.2022.105162>
- Zhang, P., Wang, J., Li, Q. F., Wan, J. Y., & Ling, Y. F. (2021). Mechanical and fracture properties of steel fiber-reinforced geopolymer concrete. *Science and Engineering of Composite Materials*, 28(1), 299-313. <https://doi.org/10.1515/secm-2021-0030>
- Zhong, H., Poon, E. W., Chen, K., & Zhang, M. Z. (2019). Engineering properties of crumb rubber alkali-activated mortar reinforced with recycled steel fibres. *Journal of Cleaner Production*, 238, 117950. <https://doi.org/10.1016/j.jclepro.2019.117950>